arXiv:1701.00025v1 [physics.flu-dyn] 30 Dec 2016

A nonmodal stability analysis of the boundary layer under solitary waves

Joris C. G. Verschaeve[1]† AND **Geir K. Pedersen**[1] AND **Cameron Tropea**[2]

[1]University of Oslo, Po.Box 1072 Blindern, 0316 Oslo, Norway
[2]Technische Universität Darmstadt, 64347 Griesheim, Germany

(Received 3 January 2017)

In the present treatise, a stability analysis based on energy bounds and nonmodal theory is performed. The instability mechanism of this flow consists of a competition between streamwise streaks and two-dimensional perturbations. For lower Reynolds numbers and early times, streamwise streaks display larger amplification due to their quadratic dependence on the Reynolds number, whereas two-dimensional perturbation become dominant for larger Reynolds numbers and later times in the deceleration region of this flow, as the maximum amplification of two-dimensional perturbations grows exponentially with the Reynolds number. By means of the present findings, the results by direct numerical simulation in (Vittori & Blondeaux 2008; Ozdemir *et al.* 2013) and experiments in (Sumer *et al.* 2010) can be explained and interpreted. In addition, three critical Reynolds numbers can be defined for which the stability properties of the flow change. In particular, it is shown that this boundary layer changes from an absolutely stable to a convectively unstable flow at a Reynolds number of $Re_\delta = 18$.

1. Introduction

In recent years, stability and transition processes in the boundary layer under solitary water waves have received increased attention in the coastal engineering community, cf. (Liu *et al.* 2007; Vittori & Blondeaux 2008; Sumer *et al.* 2010; Ozdemir *et al.* 2013; Verschaeve & Pedersen 2014). Motivated by the design of harbors and other coastal installations, this boundary layer is of importance for understanding sedimentation phenomena under water waves.

In the present treatise, the mechanisms leading to instability and finally to turbulent transition shall be investigated by means of a nonmodal stability analysis. Thereby, it shall be shown that the present boundary layer is not only of interest for the coastal engineering community, but that it also serves as a useful generic flow for the investigation of stability and transition mechanisms of aerodynamic boundary layers, such as the ones on airplane wings or on turbine blades displaying an adverse pressure gradient. In addition, the present flow can be considered a model for the single stroke of a pulsating flow, such as Stokes' second problem, which is of importance for biomedical applications.

Solitary waves, which are either found as surface or internal waves, are of great interest in the ocean engineering community for several reasons. They are nonlinear and dispersive. When frictional effects due to the boundary layer at the bottom and the top are negligible, the shape of solitary waves is preserved during propagation. Relatively simple approximate analytic solutions exists, see for instance Benjamin (1966), Grimshaw

† Email address for correspondence: joris@math.uio.no

(1971) or Fenton (1972). In addition, these waves are relatively easy to reproduce experimentally. As such, they are often used in order to investigate the effect of a single crest of a train of waves.

The first works on the boundary layer of solitary waves aimed at estimating the dissipative effect on the overall wave (Shuto 1976; Miles 1980). The bottom boundary layer has been considered more relevant (Liu & Orfila 2004) and the stability of this boundary layer is also the subject of the present treatise.

More detailed experimental and numerical work on this boundary layer and its stability properties has been performed first for the boundary layer under internal solitary waves, since this boundary layer is important for transport of sediments on the bottom of the sea (Bogucki *et al.* 1997). By means of direct numerical simulation Diamessis & Redekopp (2006) obtained a relationship for the critical parameters for which transition occurs. However, experimental results (Carr & Davies 2006, 2010) contradict this relationship, as cases deemed stable displayed instabilities and cases deemed unstable did not. More recently, a modified formula for the critical parameters has been advanced in Aghsaee *et al.* (2012) by means of direct numerical simulation.

Interest for the boundary layer under surface solitary waves has only taken off after the publication of an approximate solution to the boundary layer equations by Liu *et al.* (2007). They showed that an inflection point develops in the deceleration region behind the crest of the wave. However, instabilities have not been observed in the experiments performed by them (Liu *et al.* 2007). In 2010 Sumer *et al.* used a water tunnel to perform experiments on the boundary layer under solitary waves. They observed three flow regimes for this flow. By means of a Reynolds number Re_δ, defined by the Stokes length of the boundary layer and the characteristic particle velocity, as used in Ozdemir *et al.* (2013) and in the present treatise, these regimes can be characterized as follows. For small Reynolds numbers $Re_\delta < 630 (\approx Re_{\mathrm{Sumer}} = 2 \cdot 10^5$, i.e. the Reynolds number defined in Sumer *et al.* (2010)), the flow does not display any instabilities and is close to the laminar solution given in Liu *et al.* (2007). For a Reynolds number in the range $630 \leqslant Re_\delta < 1000$ $(2 \cdot 10^5 \leqslant Re_{\mathrm{Sumer}} < 5 \cdot 10^5)$, they observed the appearance of regularly spaced vortex rollers in the deceleration region of the flow. Increasing the Reynolds number further leads to a transitional flow displaying the emergence of turbulent spots growing together and causing transition to turbulence in the boundary layer. This happens at first in the deceleration region. However, the first instance of spot nucleation moves forward into the acceleration region of the flow for increasing Reynolds number. Sumer *et al.* did not control the level of external disturbances in their experiments nor did they report any information on its characteristics, such as length scale or intensity.

Almost parallel to the experiments by Sumer *et al.*, Vittori and Blondeaux performed direct numerical simulations of this flow (Vittori & Blondeaux 2008, 2011). Their results correspond roughly to the findings by Sumer *et al.* in that the flow in their simulations is first observed to display a laminar regime before displaying regularly spaced vortex rollers and finally becoming turbulent. However, the Reynolds numbers at which these regime shifts occur are larger than those in the experiments by Sumer *et al.*. In particular, Vittori and Blondeaux observed the flow to be laminar until a Reynolds number somewhat lower than $Re_\delta = 1000$, after which the flow in their simulations displays regularly spaced vortex rollers. Transition to turbulence has been observed to occur for Reynolds numbers somewhat larger than $Re_\delta = 1000$. The way they triggered the flow regime changes

was by introducing a random disturbance of a specific magnitude in the computational domain before the arrival of the wave. Ozdemir *et al.* (2013) performed direct numerical simulations using the same approach as Vittori and Blondeaux, but varied the magnitude of the initial disturbance. As a result they found different flow regimes than what Sumer *et al.* and Vittori and Blondeaux had observed. In the simulations by Özdemir *et al.* the flow stays laminar until $Re_\delta = 400$, then enters a regime they called 'disturbed laminar' for $400 < Re_\delta < 1500$, where instabilities can be observed. For $Re_\delta > 1500$ regularly spaced vortex rollers appear in the deceleration region of the flow in their simulations giving rise to a K-type transition before turbulent break down, if the Reynolds number is large enough. For very large Reynolds numbers $Re_{\mathrm{Sumer}} > 2400$, Özdemir *et al.* reported that the K-type transition is replaced by a transition which reminded them of a free stream layer type transition.

Next to investigations based on direct numerical simulations and experiments, modal stability theories have been employed in the works by Blondeaux *et al.* (2012) and Verschaeve & Pedersen (2014). Employing a quasi-static approach for the Orr-Sommerfeld equation, cf. (von Kerczek & Davis 1974), Blondeaux *et al.* found that this unsteady flow displayed unstable regions for all of their Reynolds number considered, even those deemed stable by direct numerical simulation.

In order to explain the divergences in transitional Reynolds numbers obtained by direct numerical simulation and experiment, Verschaeve & Pedersen (2014) performed a stability analysis in the frame of reference moving with the wave, where the present boundary layer flow is steady. For steady flows, well-established stability methods can be used. By means of the parabolized stability equation, they showed that for all Reynolds numbers considered in their analysis, the boundary layer displays regions of growth of disturbances. As the flow goes to zero towards infinity, there exists a point in time where the perturbations reach a maximum amplification before decaying again for a given Reynolds number. Depending on the level of initial disturbances in the flow, this maximum amount of amplification is sufficient for triggering secondary instability or not. This explains the diverging critical Reynolds numbers observed in direct numerical simulations and experiments for this boundary layer flow. A particular case in point, mentioned in Verschaeve & Pedersen (2014), is the experiment on the boundary layer under internal solitary waves by Carr & Davies (2006, 2010). In these experiments, the flow displays instabilities for Reynolds numbers much smaller than in the experiments by Sumer *et al.* (2010) or in the direct numerical simulations by Vittori & Blondeaux (2008) or Ozdemir *et al.* (2013), although these boundary layer flows are very similar in the limit of small amplitude solitary waves. Verschaeve & Pedersen (2014) proposed, that due to the characteristic velocity of internal solitary waves being significantly smaller than that for surface solitary waves, they are expected to display instabilities much earlier for comparable levels of background noise.

The modal stability theories employed in Blondeaux *et al.* (2012) and Verschaeve & Pedersen (2014) capture only parts of the picture. In both works, only two-dimensional disturbances are considered. In addition, the amplifications computed in Verschaeve & Pedersen (2014) describe only the so-called exponential growth of the most unstable eigenfunction of the Orr-Sommerfeld equation. As shown in Butler & Farrell (1992); Trefethen *et al.* (1993); Schmid & Henningson (2001); Schmid (2007), perturbations can undergo significant transient growth even when modal stability theories predict the flow system to be stable. Nonmodal theory formulates the stability problem as an optimization problem for the perturbation energy. In the present treatise, optimal perturbations are

computed for the unsteady boundary layer flow under a solitary wave, complementing the modal analysis performed in (Blondeaux *et al.* 2012; Verschaeve & Pedersen 2014). In particular, we shall investigate the following questions.

In (Verschaeve & Pedersen 2014), the stability of the flow has been analyzed for a wide range of Reynolds numbers. For all these Reynolds numbers considered the flow displayed regions of instability. However, can a critical Reynolds number $Re_A > 0$ be found, such that for all Reynolds numbers smaller than Re_A, the flow is absolutely stable, meaning that all perturbations are damped for all times? Using the energy bound derived in (Davis & von Kerczek 1973), we shall show in the following that such a critical Reynolds number exists, which makes this boundary layer one of the few examples of a flow displaying an inflection point in the velocity profile but being absolutely stable.

Ozdemir *et al.* (2013) supposed that a by-pass transition starts to develop in their simulations for some cases, but could not explain why then suddenly two-dimensional perturbations emerge producing a K-type transition typical for growing Tollmien-Schlichting waves. In the present treatise, we shall show that nonmodal theory is able to describe this competition between streaks and two-dimensional perturbations (i.e. nonmodal Tollmien-Schlichting waves), allowing to predict the onset of growth of streaks and two-dimensional perturbations, their maximum amplification and the point in time when this maximum is reached. Furthermore, the dependence on the Reynolds number of the maximum amplification shall be investigated. The results obtained in the present treatise explain why in the direct numerical simulations by Vittori & Blondeaux (2008, 2011) and Ozdemir *et al.* (2013), in all cases two dimensional perturbations lead to turbulent break-down, although one would expect, at least for some cases, turbulent break-down via three dimensional structures for a purely random seeding. On the other hand Sumer *et al.* (2010) observed the growth of two-dimensional structures only for a certain range of Reynolds numbers, before the appearance of turbulent spots. A K-type transition has not been observed in their experiments. Turbulent spots are in general attributed to the secondary instability of streamwise streaks, see for example (Andersson *et al.* 2001; Brandt *et al.* 2004). Though, the random break-down of Tollmien-Schlichting waves is also thought to produce turbulent spots, cf. (Shaikh & Gaster 1994; Gaster 2016). The present analysis is limited to the primary instability of streamwise streaks and nonmodal Tollmien-Schlichting waves. It gives, however, indications for a possible secondary instability mechanism of competing streaks and Tollmien-Schlichting waves.

The present treatise is organized as follows. In the following section, section 2, we describe the flow system and present equations for energy bounds and the nonmodal governing equations. The solutions of these equations applied to the present flow are presented and discussed in section 3. In this section, we shall also relate the current findings to results obtained previously in the literature. The present treatise is concluded in section 4.

2. Description of the problem

2.1. *Specification of base flow*

The outer flow of the present boundary layer is given by the celebrated first order solution for the inviscid horizontal velocity for solitary waves (Benjamin 1966; Fenton 1972). For a given point at the bottom, the outer flow can thus be written as in Sumer *et al.* (2010):

$$U^*_{\text{outer}}(t^*) = U_0 \text{sech}^2\left(\omega_0 t^*\right). \tag{2.1}$$

In the limit of vanishing amplitude of the solitary wave, not only the nonlinearities in the inviscid solution become negligible, but they can also be neglected in the boundary layer equations. Following Liu & Orfila (2004), the horizontal component in the boundary layer U_{base} can be written as

$$U_{\text{base}} = U_{\text{outer}} + u_{bl}, \tag{2.2}$$

where u_{bl} contains the rotational part of the velocity and ensures that the no-slip boundary condition is satisfied. Neglecting the nonlinearities, we obtain the following boundary layer equations for u_{bl} (Liu *et al.* 2007; Park *et al.* 2014):

$$\frac{\partial}{\partial t}u_{bl} = \frac{1}{2}\frac{\partial^2}{\partial z^2}u_{bl} \tag{2.3}$$

$$u_{bl}(0,t) = -U_{\text{outer}}(t) \tag{2.4}$$

$$u_{bl}(\infty,t) = 0 \tag{2.5}$$

$$u_{bl}(z,-\infty) = 0 \tag{2.6}$$

The scaling used in equations (2.3-2.6) is given by ω_0 for the time,

$$t = \omega_0 t^*, \tag{2.7}$$

by U_0 for the velocity,

$$U_{\text{outer}} = \frac{1}{U_0}U^*_{\text{outer}}, \tag{2.8}$$

and by the Stokes length δ for the wall normal variable z:

$$z = \frac{z^*}{\delta}, \tag{2.9}$$

where

$$\delta = \sqrt{\frac{2\nu}{\omega_0}}, \tag{2.10}$$

is the Stokes length. For the solution of equations (2.3-2.6), a Chebyshev collocation discretization in wall normal direction and a Crank-Nicolson scheme in time is employed.

2.2. *Stability analysis by means of an energy bound*

In the present treatise, we use the same definition for the Reynolds number as in Ozdemir *et al.* (2013). This Reynolds number Re_δ is based on the Stokes length δ and the characteristic velocity U_0:

$$Re_\delta = \frac{U_0\delta}{\nu} = U_0\sqrt{\frac{2}{\nu\omega_0}}, \tag{2.11}$$

where ν is the kinematic viscosity of the fluid. The Reynolds number Re_{Sumer} used in Sumer *et al.* (2010) is related to Re_δ by the following formula:

$$Re_\delta = \sqrt{2Re_{\text{Sumer}}}. \tag{2.12}$$

The time τ in the resulting Navier-Stokes equations is then scaled the following way:

$$\tau = \frac{U_0}{\delta}t^* = \frac{Re_\delta}{2}t. \tag{2.13}$$

We introduce a perturbation velocity $\mathbf{u}' = (u', v', w')$ in the streamwise, spanwise and wall normal direction, defined by:

$$\mathbf{u}' = (u', v', w') = (u_{ns}, v_{ns}, w_{ns}) - (U_{\text{base}}(z, \tau\frac{2}{Re_\delta}), 0, 0), \tag{2.14}$$

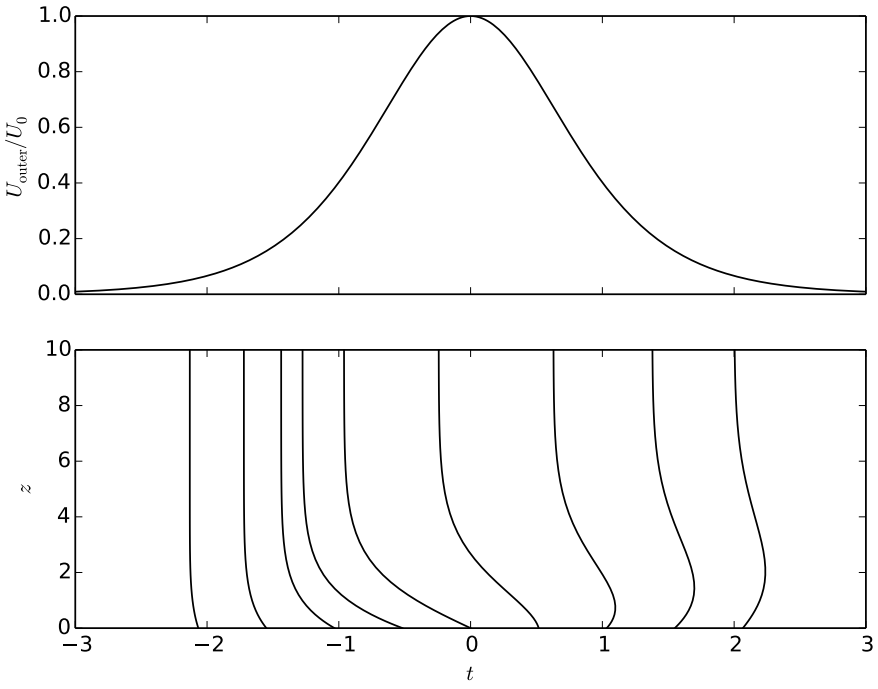

Figure 1: Inviscid outer flow U_{outer} at the bottom and profiles of the horizontal velocity component in the boundary layer under a solitary wave moving from right to left. The profiles have been multiplied by 40. The value at $z = 0$ of the profiles shown corresponds to the point in time t, at which the profile has been taken. The horizontal velocity vanishes at $z = 0$ in order to satisfy the no-slip boundary condition.

where (u_{ns}, v_{ns}, w_{ns}) satisfies the Navier-Stokes equations. The energy of the perturbation is given by:

$$E_p = \int_V u'^2 + v'^2 + w'^2 \, dV, \tag{2.15}$$

which is integrated over $V = \{(x, y, z) \,|\, z > 0\}$. For time dependent flows in infinite domains, Davis & von Kerczek (1973) derived a bound for the perturbation energy of the nonlinear Navier-Stokes equations:

$$\frac{E_p(\tau)}{E_{p,0}} \leqslant \exp \int_{\tau_0}^{\tau} \mu(\tau') \, d\tau', \tag{2.16}$$

where μ is the largest eigenvalue of the following linear system:

$$\frac{1}{Re_\delta} \Delta \mathbf{u}' - \mathbf{S}_{\text{base}}(\tau) \cdot \mathbf{u}' - \nabla p = \frac{1}{2} \mu \mathbf{u}' \tag{2.17}$$

$$\nabla \cdot \mathbf{u}' = 0, \tag{2.18}$$

where the tensor $\mathbf{S}_{\text{base}}$ is the rate of strain tensor given by the base flow, equation (2.2). We remark that Davis & von Kerczek (1973) lost a sign and a factor two in their

equations. As the rate of strain tensor depends on time, the eigenvalue μ is a function of τ. If $\mu < 0$ for all times, then the flow is absolutely stable for this Reynolds number, meaning that all perturbations will decay for all times. This allows us to investigate, if there exists a Reynolds number Re_A, at which μ switches sign from negative to positive at some point in time. As the base flow is independent of x and y, we consider a single Fourier component of $\mathbf{u}'$:

$$(u', v', w')(x, y, z, \tau) = (u, v, w)(z, \tau) \exp \mathrm{i}\,(\alpha x + \beta y)\,. \tag{2.19}$$

This allows us to eliminate p from the equations (2.17-2.18), resulting into

$$\frac{1}{Re_\delta}\mathcal{L}^2 w + \frac{\mathrm{i}\alpha}{2}\left\{\frac{\partial^2}{\partial z^2}U_{\mathrm{base}} w + 2\frac{\partial}{\partial z}U_{\mathrm{base}}\frac{\partial}{\partial z} w\right\} + \frac{\mathrm{i}\beta}{2}\frac{\partial}{\partial z}U_{\mathrm{base}}\zeta = \frac{1}{2}\mu\mathcal{L}w, \tag{2.20}$$

$$-\frac{1}{Re_\delta}\mathcal{L}\zeta - \frac{\mathrm{i}\beta}{2}\frac{\partial}{\partial z}U_{\mathrm{base}} w = \frac{1}{2}\mu(-\zeta) \tag{2.21}$$

where $\mathcal{L}$ is the Laplacian defined by:

$$\mathcal{L} = -k^2 + \frac{\partial^2}{\partial z^2}, \tag{2.22}$$

where $k^2 = \alpha^2 + \beta^2$. The system of four equations (2.17-2.18), has been reduced to two, by means of the normal vorticity component ζ:

$$\zeta = \mathrm{i}\,(\alpha v - \beta u)\,. \tag{2.23}$$

A Galerkin formulation for the system (2.20-2.21) is chosen based on Shen-Legendre polynomials for the biharmonic equation for the normal component w and Shen-Legendre polynomials for the Poisson equation for the normal vorticity ζ, cf. reference (Shen 1994). Thereby, the Hermitian property of the system (2.20-2.21) is conserved in the discrete setting, guaranteeing purely real eigenvalues. Details of the implementation are given in appendix A.

2.3. *The nonmodal stability equations*

The nonmodal stability analysis is based on the linearized Navier-Stokes equations, which can be written in the present setting as follows,

$$\left(\partial_\tau + \mathrm{i}\alpha U_{\mathrm{base}} - \frac{1}{\mathrm{Re}_\delta}\mathcal{L}\right)\mathcal{L}w - \mathrm{i}\alpha w\frac{\partial^2}{\partial z^2}U_{\mathrm{base}} = 0, \tag{2.24}$$

$$\left(\partial_\tau + \mathrm{i}\alpha U_{\mathrm{base}} - \frac{1}{\mathrm{Re}_\delta}\mathcal{L}\right)\zeta - \mathrm{i}\beta w\frac{\partial}{\partial z}U_{\mathrm{base}} = 0. \tag{2.25}$$

We refer to Schmid & Henningson (2001); Schmid (2007) for a thorough derivation of equations (2.24) and (2.25). We remark that U_{base} varies on the convective time scale in equations (2.24) and (2.25):

$$U_{\mathrm{base}} = U_{\mathrm{base}}\left(z, \tau\frac{2}{Re_\delta}\right). \tag{2.26}$$

Given an initial perturbation (w_0, ζ_0) at time τ_0, equations (2.24) and (2.25) can be integrated to obtain the temporal evolution of (w, ζ) for $\tau > \tau_0$. Nonmodal theory formulates the stability problem as finding the initial condition (w_0, ζ_0) maximizing the perturbation energy $E(\tau)$ of (w, ζ) at time $\tau > \tau_0$. This perturbation energy E is the sum of two contributions, one from the wall normal component w and one from the normal vorticity

component ζ:

$$E(\tau) = E_w(\tau) + E_\zeta(\tau) = \frac{1}{2}\int_0^\infty \frac{1}{k^2}\left|\frac{\partial}{\partial z}w\right|^2 + |w|^2\, dz + \frac{1}{2}\int_0^\infty \frac{1}{k^2}|\zeta|^2\, dz. \tag{2.27}$$

The optimization problem can then be formulated by maximizing E for a perturbation (w, ζ) satisfying (2.24) and (2.25) and having an initial energy E_0. One way of solving this optimization problem is by means of the adjoint equation as in Luchini & Bottaro (2014). Another approach for finding the optimal perturbation, which is employed in the present treatise, consists in formulating the discrete problem first and computing the evolution matrix $\mathbf{X}(\tau, \tau_0)$ of the system of ODEs, cf. references Trefethen *et al.* (1993); Schmid & Henningson (2001); Schmid (2007) for details. The energy E is then given in terms of $\mathbf{X}$ and the initial condition. Details of the implementation are given in appendix A. By computing $E(\tau)$ one way or the other, we can compute the amplification A from time τ_0 to τ of the optimal perturbation for wave numbers α and β:

$$A(\alpha, \beta, \tau_0, \tau, Re_\delta) = \max_{(w_0,\zeta_0)} \frac{E(\tau)}{E(\tau_0)}. \tag{2.28}$$

The maximum amplification $A_{\max}(Re_\delta)$, which can be reached for a given Reynolds number Re_δ, is obtained by maximizing A over time, initial time and wavenumbers:

$$A_{\max} = \max_{\alpha,\beta,\tau_0,\tau} A. \tag{2.29}$$

In the following, we shall distinguish between three types of perturbations:

- streamwise streaks.

These are perturbations independent of the streamwise coordinate x. They can be computed by setting $\alpha = 0$.

- Two-dimensional perturbations.

These perturbations are independent of the spanwise coordinate y and can be computed by setting $\beta = 0$. In this case, equations (2.24) and (2.25) are decoupled. These two-dimensional perturbations can be considered nonmodal Tollmien-Schlichting waves resulting from an optimization of the initial conditions of (2.24) and (2.25). Therefore, they display larger growth than modal Tollmien-Schlichting waves resulting from the Orr-Sommerfeld equation. This shall be presented more in detail in section 3.

- Oblique perturbations.

These are all remaining perturbations with $\alpha \neq 0$ and $\beta \neq 0$.

3. Results and discussion

3.1. *Absolute stability*

In this section, we shall determine the critical Reynolds number Re_A behind which perturbations display growth. To this aim, the energy criterion in Davis & von Kerczek (1973) shall be used. We solve equations (2.20) and (2.21) for a given pair of wave numbers (α, β) and note the Reynolds number Re_δ for which the largest eigenvalue μ changes from minus to plus. At first, we compute the curves of critical Reynolds numbers $Re_\delta(\alpha)$ and $Re_\delta(\beta)$ by setting $\beta = 0$ and $\alpha = 0$, respectively. These curves are plotted in figure 2. As it turns out, all other cases, i.e. $\alpha \neq 0$ and $\beta \neq 0$, have their critical Reynolds number lying in the region between these two curves. From figure 2, we can infer that the flow is absolutely stable for all Reynolds numbers Re_δ smaller than $Re_A = 18$. The physical

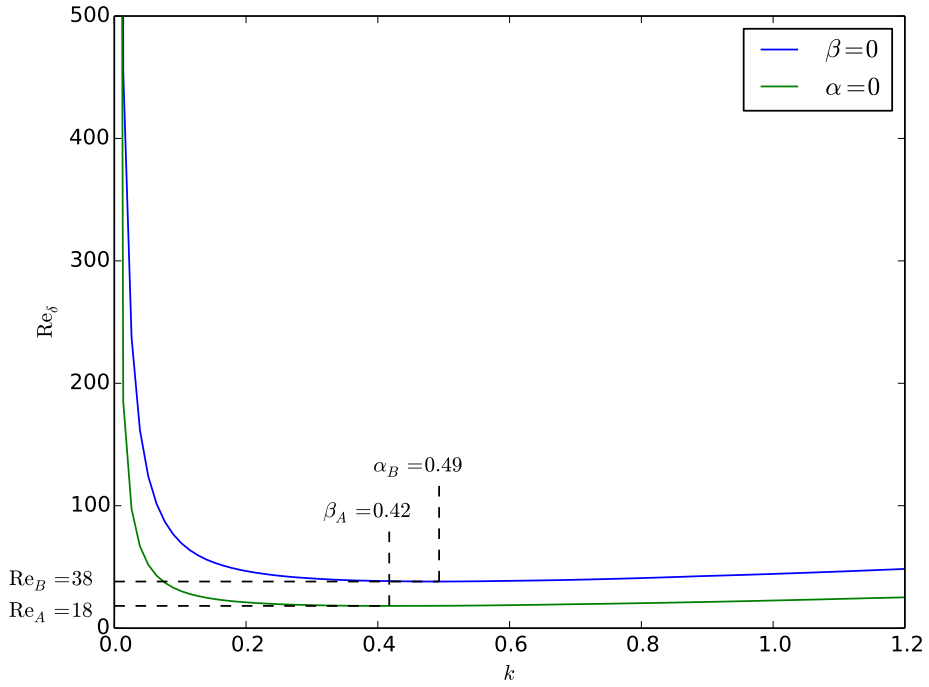

Figure 2: Isolines of $\mu = 0$ for the energy bound of Davis & von Kerczek (1973), equations (2.20) and (2.21), as a function of the wave number $k^2 = \alpha^2+\beta^2$ and the Reynolds number Re_δ. The blue and green lines correspond to the cases $\beta = 0$ and $\alpha = 0$, respectively. All other cases have their critical Reynolds number in the space between these lines.

significance of this critical Reynolds number is, however, limited. For example, the water depth of a surface solitary wave with amplitude ratio $\epsilon = 0.1$ would be approximately 1 cm for this case. For these small water depths, other physical effects, such as capillary effects and not least the dissipative effect of the boundary layers on the solitary wave, are not negligible anymore. The solitary wave solution would thus not be valid in the first place. However, the present flow is an illustrative example when considering the lower range of validity of Rayeleigh's inflexion point theorem or Fjørtoft's theorem for inviscid flows (Drazin & Reid 1981). Another example of such a flow is the related case of Stokes second problem, for which Davis & von Kerczek (1973) computed the corresponding critical Reynolds number. From figure 2, we observe that streamwise streaks will grow first. Two-dimensional perturbations, on the other hand, will only grow for flows with a Reynolds number larger than $Re_B = 38$.

3.2. *Optimal perturbation*

Before turning to the computation of the amplification A, equation (2.28), we shall first consider a scaling argument, as in Gustavsson (1991); Schmid & Henningson (2001). For

streamwise streaks ($\alpha = 0$), equations (2.24) and (2.25) can be written as:

$$\left(\partial_t - \frac{1}{2}\mathcal{L}\right)\mathcal{L}\tilde{w} = 0, \tag{3.1}$$

$$\left(\partial_t - \frac{1}{2}\mathcal{L}\right)\tilde{\zeta} - \mathrm{i}\beta\tilde{w}\frac{\partial}{\partial z}U_{\mathrm{base}}\,(z,t) = 0, \tag{3.2}$$

where $\tilde{w}$ depends now on t and $\tilde{\zeta}$ is in addition scaled by $Re_\delta/2$:

$$\tilde{\zeta} = \frac{2}{Re_\delta}\zeta(z,t). \tag{3.3}$$

From equations (3.1) and (3.2), we can infer that for streamwise streaks w and ζ display temporal variations on a convective time scale. As for steady flows (Gustavsson 1991; Schmid & Henningson 2001), the energy E_ζ is proportional to the square of the Reynolds number for the present unsteady flow:

$$E_\zeta \propto Re_\delta^2. \tag{3.4}$$

For large Reynolds numbers E_ζ will dominate. Therefore, the maximum amplification A for streamwise streaks is expected to behave as

$$\max_{\beta,t_0,t} A(\alpha = 0, \beta, t_0, t, Re_\delta) \approx Re_\delta^2 \quad Re_\delta >> 1. \tag{3.5}$$

On the other hand, for two-dimensional perturbations ($\beta = 0$), when neglecting viscous dissipation, equation (2.24) can be written:

$$\frac{\partial}{\partial t}\mathcal{L}w = \mathrm{i}\alpha Re_\delta\frac{1}{2}\left(\frac{\partial^2}{\partial z^2}U_{\mathrm{base}} - U_{\mathrm{base}}\mathcal{L}\right)w. \tag{3.6}$$

We might therefore argue that in our case, for large Re_δ, the maximum amplification for two-dimensional perturbations roughly behaves like:

$$\max_{\alpha,t_0,t} A(\alpha, \beta = 0, t_0, t, Re_\delta) \approx e^{cRe_\delta}, \tag{3.7}$$

where c is some constant. In the following, we shall see that the competition of the maximum amplification between the quadratic growth in Re_δ of streamwise streaks, equation (3.5), and the exponential growth in Re_δ of two-dimensional structures, equation (3.7), composes the essential instability mechanism of this flow.

The amplification A, equation (2.28), for the present flow problem depends on five parameters, the wavenumbers α and β, the initial time t_0, the time t and the Reynolds number Re_δ. We start our analysis by tracing the evolution of $\max_{\alpha,\beta} A$ for a given Reynolds number Re_δ and a given initial time t_0. In figure 3, we plot the temporal evolution of $\max_{\alpha,\beta} A$ for the Reynolds numbers $Re_\delta = 141, 316, 447$ and 1000 ($Re_{\mathrm{Sumer}} = 10^4, 5\cdot 10^4, 10^5, 5\cdot 10^5$) and initial times $t_0 = -8, -6, \ldots, 6$. For the case $Re_\delta = 141$, cf. figure 3a, we observe that growth of perturbations is mainly restricted to the deceleration region of the flow, i.e. where $t > 0$. Only the optimal perturbation starting at $t_0 = -2$ displays some growth before the arrival of the crest of the solitary wave. Among the initial conditions t_0 chosen, the optimal perturbation with $t_0 = 0$ displays the maximum amplification at $t_{\max} = 1.5$ with $A \approx 20$. This is due to the acceleration region of the flow ($t < 0$) having a damping effect on the perturbations starting before $t = 0$. On the other hand the perturbations starting at later times $t_0 \geqslant 2$ already miss out a great deal of the destabilizing effect of the adverse pressure gradient. All curves display a maximum

at some time. For some cases, this maximum lies outside of the plotting domain. For a slightly larger Reynolds number, cf. figure 3b with $Re_\delta = 316$, we observe a qualitatively similar behavior for the perturbations starting at $t_0 < 0$ with the difference that growth of these perturbations sets in somewhat earlier in time than in the $Re_\delta = 141$ case and leads also to higher amplifications. However, the optimal perturbation starting at $t_0 = 0$ behaves differently than the corresponding one for the $Re_\delta = 141$ case. At early times, i.e. for $t \lesssim 2$, the evolution of this perturbation is similar to the $Re_\delta = 141$ case. The perturbation grows to a maximum $A \approx 100$ at $t \approx 1.5$, before decaying again, but, at time $t \approx 2$, the amplification curve displays a kink and a sudden growth to $A \approx 2000$ at time $t_{\max} = 8.2$. A similar, however, less expressive kink is also visible in the curve for $t_0 = 2$. Increasing the Reynolds number to $Re_\delta = 447$, cf. figure 3c, does not change the picture qualitatively. However, the maximum amplification of the optimal perturbation starting at $t_0 = 0$ has increased by a factor of approximately thousand compared to the $Re_\delta = 316$ case. In comparison, the maximum of the optimal perturbation starting at $t_0 = -2$ has only increase by a factor of approximately 1.25 when going from $Re_\delta = 316$ to $Re_\delta = 447$. This violent growth for the optimal perturbation starting at t_0 is also visible for the $Re_\delta = 1000$ case, cf. figure 3d. However, for this case, even the curves of the perturbations starting at earlier times display a similar kink and sudden growth in the deceleration region.

In figure 4, we plot contour plots of the amplification $A(\alpha, \beta, t_0 = 0, t_{\max}, Re_\delta)$ at $t_{\max} = 1.5, 8.2, 9.9, 16.5$ for the cases $Re_\delta = 141, 316, 447, 1000$, respectively. For the case $Re_\delta = 141$, cf. figure 4a, we find a single maximum lying on the β-axis. On the other hand, the $Re_\delta = 316$ case is different, cf. figure 8a. Whereas all two-dimensional perturbations display decay at $t_{\max} = 1.5$ for the $Re_\delta = 141$ case, the amplification of two-dimensional perturbations displays a peak at around $\alpha = 0.35$ for the $Re_\delta = 316$ case. A second peak, lying on the β axis, is significantly smaller than the peak of two-dimensional perturbations on the α-axis. Increasing the Reynolds number, cf. figures 8b and 4d, increases the magnitude of the peaks, with the peak on the α-axis growing faster with Re_δ than the peak on the β-axis. This competition between streamwise streaks and two-dimensional structures is characteristic for flows with adverse pressure gradients and has also been observed for steady flows. The Falkner-Skan boundary layer with adverse pressure gradient displays contour levels similar to the present ones, cf. for example Levin & Henningson (2003, figure 10d) or Corbett & Bottaro (2000). Another example is the flow of three dimensional swept boundary layers investigated in Corbett & Bottaro (2001).

The competition between streamwise streaks and two-dimensional perturbations can also be observed in the temporal evolution of the amplification of the optimal perturbation. In figure 5, we compare the temporal evolution of $\max_\beta A(\alpha = 0, \beta, t_0 = 0, t, Re_\delta = 316)$, $\max_\alpha A(\alpha, \beta = 0, t_0 = 0, t, Re_\delta = 316)$ and $\max_{\alpha,\beta} A(\alpha, \beta, t_0 = 0, t, Re_\delta = 316)$. For early times ($0 < t \lesssim 2$) the streamwise streaks display a larger amplification than the two-dimensional perturbations, but at time $t \approx 2$, the two-dimensional perturbations overtake the streaks. Maximizing over α and β, chooses either perturbation displaying maximum amplification. The amplification of oblique perturbations seems to be always smaller than that of streamwise streaks or two-dimensional perturbations. This allows us to trace the maximum amplification $A_{\max}$, equation (2.29), by considering only the amplification of the cases $(\alpha = 0, \beta)$ and $(\alpha, \beta = 0)$ instead of maximizing over all possible wave numbers (α, β). In figure 6, the amplification of streamwise streaks and two-dimensional perturbations maximized over the initial time t_0 and time t is plotted against the Reynolds number. As predicted in section 3.1 by the energy bound of Davis & von Kerczek (1973), streamwise streaks start to grow for Reynolds numbers larger than

$Re_A = 18$, whereas two-dimensional perturbations start growing after $Re_B = 38$. We can define a third critical Reynolds number $Re_C = 170$ for this flow, which stands for the moment when the maximum amplification of two-dimensional perturbations overtakes the maximum amplification of streamwise streaks. This happens for rather low levels of amplification, the maximum amplification being $A_{\max} = 28$ for $Re_\delta = 170$. For flows with a Reynolds number larger than Re_C, which are most relevant cases, the dominant perturbations are likely to be two-dimensional (up to secondary instability). This supports the observation by Vittori & Blondeaux (2008) and Ozdemir *et al.* (2013) of a transition process via the development of two-dimensional vortex rollers. However, when starting early, i.e. for initial times $t_0 < -1$, streamwise streaks start growing before two-dimensional structures, as can be seen in figure 3d. The competition between streamwise streaks and two-dimensional structures to first reach secondary instability, might therefore not only be determined by the maximum amplification reached, but also by the point in time, when the amplification of the perturbation is sufficient to trigger secondary instability, be it streaks or two-dimensional perturbations. We shall discuss this point further in section 3.3.

When plotting the maximum amplification of streamwise streaks in a log-log plot, cf. figure 7, we find the expected quadratic behavior of the maximum amplification. The scaling properties of streamwise streaks can also be observed in the initial condition for the optimal streak with maximum amplification, cf. figure 8. We observe that for larger Reynolds numbers, the graphs of $|w| \cdot Re_\delta$ and $|\zeta|$ collapse. A similar collapse for the initial condition of the two-dimensional perturbation with maximum amplification can be seen in figure 9.

3.3. *Relation to previous results in the literature*

A question which suggest itself immediately, is the relation between the present non-modal stability analysis and the modal stability analyses performed previously in Blondeaux *et al.* (2012) and Verschaeve & Pedersen (2014). Naturally, the amplifications of the optimal perturbations are expected to be larger than the corresponding ones of the modal Tollmien-Schlichting waves. This can be seen in figure 10, where we have solved the Orr-Sommerfeld equation for the present problem in a quasi-static fashion for the wave number $\alpha = 0.35$ and Reynolds numbers $Re_\delta = 141$ and 447. The amplification of the optimal perturbation can be several orders of magnitude larger than that of the corresponding modal Tollmien-Schlichting wave. On the other hand the main conclusions by Verschaeve & Pedersen (2014) are still supported by the present analysis. Although attempted by several experimental and direct numerical studies (Vittori & Blondeaux 2008; Sumer *et al.* 2010; Ozdemir *et al.* 2013; Diamessis & Redekopp 2006; Carr & Davies 2006, 2010; Aghsaee *et al.* 2012), a well defined transitional Reynolds number cannot be given for this flow. As also pointed out in the present analysis, depending on the characteristics of the exterior perturbations, such as length scale and intensity, the flow might transition to turbulence for different Reynolds numbers. Without control of the exterior perturbations, any experiment on the stability properties of this flow will hardly be repeatable. On the other hand, as we have shown above, a critical Reynolds number Re_A can be defined, for which the present flow switches from an absolutely stable to a convectively unstable flow. This critical Reynolds number has, however, little practical bearing.

Concerning the direct numerical simulations by Vittori & Blondeaux (2008, 2011) and Ozdemir *et al.* (2013), the present study gives an explanation for the transition process happening via two-dimensional vortex rollers observed in their direct numerical simula-

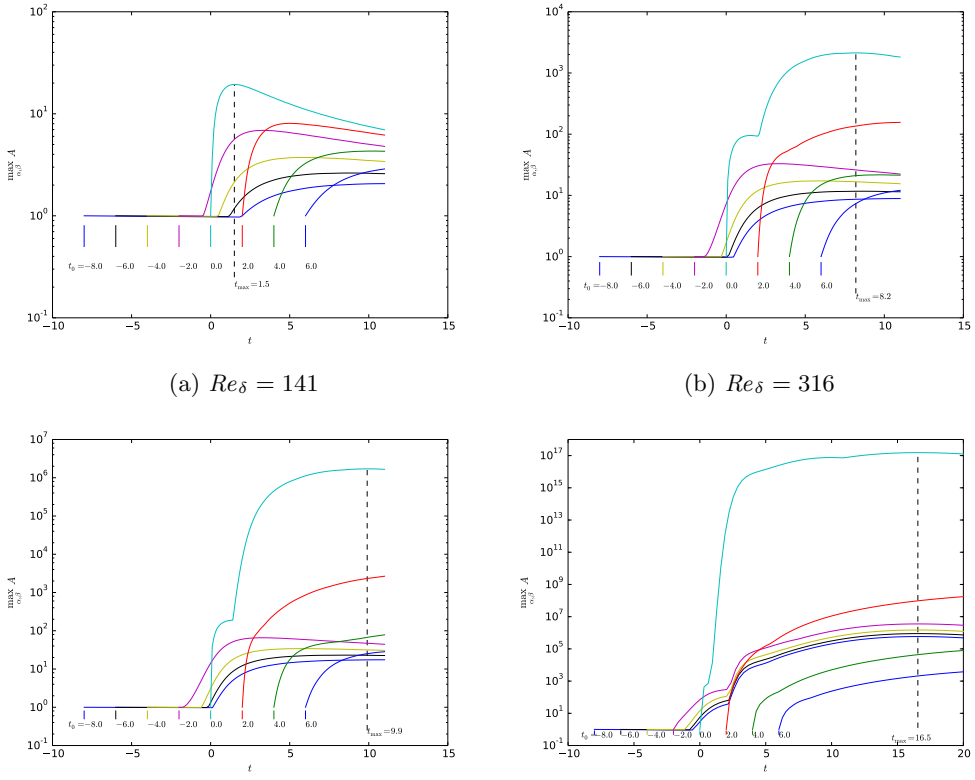

(a) $Re_\delta = 141$ (b) $Re_\delta = 316$

(c) $Re_\delta = 447$ (d) $Re_\delta = 1000$

Figure 3: Temporal evolution of the amplification A maximized over the wavenumbers α and β for different Reynolds numbers Re_δ and initial times t_0.

tions. In addition, we are able to answer the question raised by Ozdemir *et al.* (2013) about the possible mechanism of a by-pass transition. However, quantitative differences between the direct numerical results by Ozdemir *et al.* (2013) and the present ones exist. Ozdemir *et al.* (2013) introduce a random disturbance at $t_0 = -\pi$ with different amplitudes in their simulations and monitor the evolution of the amplitude of these disturbances, cf. figure 10 in Ozdemir *et al.* (2013). From this figure, we see the characteristic kink of two-dimensional perturbations overtaking streamwise streaks appearing in their simulations only for $Re_\delta = 2000$ and higher. If we compare this to the optimal perturbations with initial times $t_0 = -4$ and $t_0 = -2$ in figure 3, we see this kink developing already for a much lower Reynolds number, namely $Re_\delta = 1000$, cf. figure 3d. The reasons for this discrepancy are unclear. We might, however, point out that, in order for a Navier-Stokes solver to capture the growth of two-dimensional perturbations correctly an extremely fine resolution in space and time is needed, as can be seen in Verschaeve & Pedersen (2014, Appendix A) for modal Tollmien-Schlichting waves. In particular, when the resolution requirements are not met, these perturbations tend to be damped instead of amplified. In this respect, it is interesting to note, that Vittori & Blondeaux (2008, 2011) found that regular vortex tubes appeared in their simulation for a Reynolds number around $Re_\delta = 1000$ ($Re_{\text{Sumer}} = 5 \cdot 10^5$), which corresponds relatively well with the present findings.

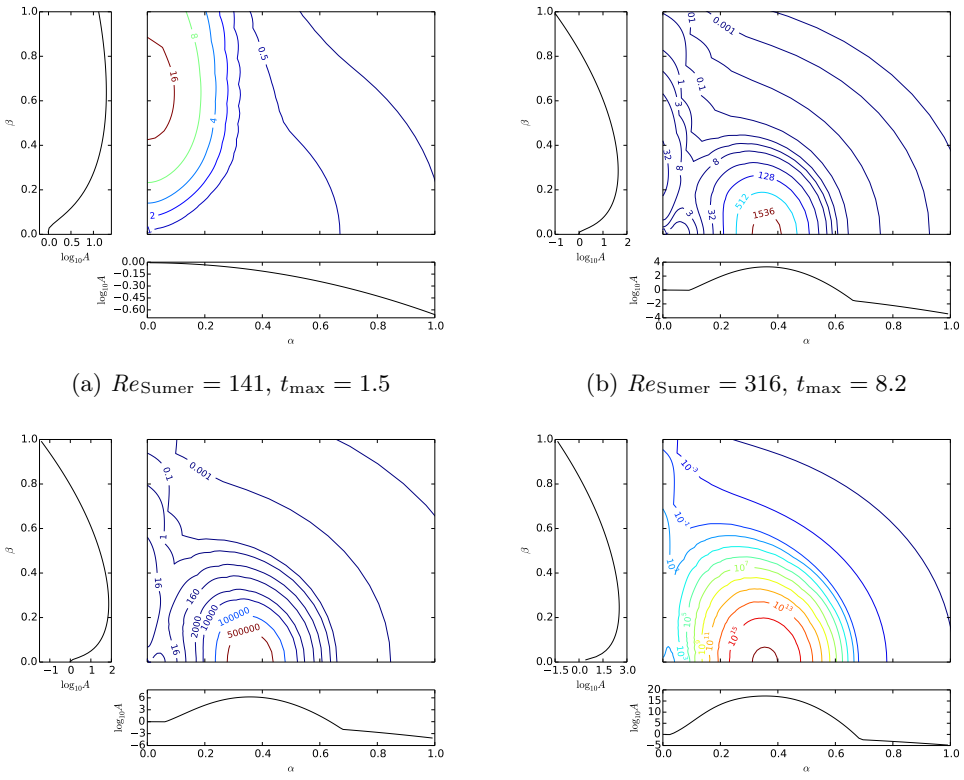

(a) $Re_{\mathrm{Sumer}} = 141$, $t_{\max} = 1.5$

(b) $Re_{\mathrm{Sumer}} = 316$, $t_{\max} = 8.2$

(c) $Re_{\mathrm{Sumer}} = 447$, $t_{\max} = 9.9$

(d) $Re_{\mathrm{Sumer}} = 1000$, $t_{\max} = 16.5$

Figure 4: Contour plots of the amplification $A(\alpha, \beta, t_0 = 0, t_{\max}, Re_\delta)$ at $t_{\max} = 1.5, 8.2, 9.9, 16.5$ for the cases $Re_\delta = 141, 316, 447, 1000$, respectively. The plots to the left and below the contour plot show a slice along the β- and α-axes, respectively.

In the experiments by Sumer *et al.* (2010) the vortex rollers appeared in the range $630 \leqslant Re_\delta < 1000$. Assuming that the initial level of external perturbations in the experiments is higher than in the direct numerical simulations, the observation by Sumer *et al.* fits the present picture. However, for $Re_\delta > 1000$, they observed the development of turbulent spots in the deceleration region of the flow. This is in contrast to the results by Ozdemir *et al.* (2013) of a K-type transition The present analysis supports the finding of a transition process via the growth of two-dimensional perturbations. However, whether these nonmodal Tollmien-Schlichting waves break down via a K-type transition as in Ozdemir *et al.* (2013) or whether they break up randomly producing turbulent spots (Shaikh & Gaster 1994; Gaster 2016) is difficult to say from this primary instability analysis. In addition, more information on the initial disturbances in the experiments is needed to make any conclusions. Whereas random noise is applied in Vittori & Blondeaux (2008, 2011) and Ozdemir *et al.* (2013), the initial disturbance in Sumer *et al.* (2010) might be free stream turbulence of certain characteristics. Depending on these characteristics, other perturbations than the one showing optimal amplification, might induce secondary instability. In addition, it cannot be excluded that a completely different instability mechanism is at work in the experiments of Sumer *et al.* (2010). The focus in the present analysis is on the response to initial conditions and does not take into ac-

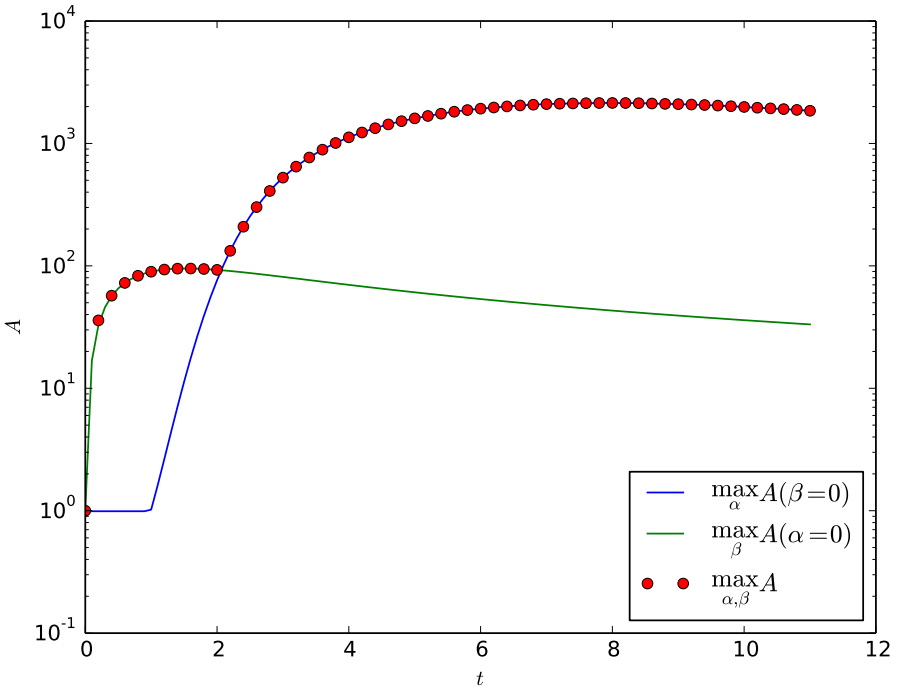

Figure 5: Temporal evolution of $\max_\beta A(\alpha = 0, \beta, t_0 = 0, t, Re_\delta = 316)$, $\max_\alpha A(\alpha, \beta = 0, t_0 = 0, t, Re_\delta = 316)$ and $\max_{\alpha,\beta} A(\alpha, \beta, t_0 = 0, t, Re_\delta = 316)$.

count any response to external forcing, which would be modeled by adding a source term to the equations (2.24) and (2.25). It is possible that the present flow system displays some sensitivity to certain frequencies of vibrations present in the experimental set-up altering the behavior of the system for larger Reynolds numbers. In particular, different perturbations, such as streamwise streaks, might be favored, leaving the possibility open that the turbulent spots, nevertheless, result from the break-down of streamwise streaks (Andersson *et al.* 2001; Brandt *et al.* 2004).

4. Conclusions

In the present treatise, a nonmodal stability analysis of the bottom boundary layer flow under solitary waves is performed. Two competing mechanism can be identified: Growing streamwise streaks and growing two-dimensional perturbations (nonmodal Tollmien-Schlichting waves). By means of an energy bound, it is shown that the present flow is absolutely stable for Reynolds numbers below $Re_\delta = 18$ after which it turns convectively unstable, with streamwise streaks growing first. Two-dimensional perturbations display growth only for Reynolds numbers larger than $Re_\delta = 38$. However, their maximum amplification overtakes that of streamwise streaks at $Re_\delta = 170$. As for steady flows, the maximum amplification of streamwise streaks displays quadratic growth with Re_δ for the present unsteady flow. On the other hand, the maximum amplification of two-dimensional perturbations shows a near exponential growth in the deceleration region of the flow. Therefore, the dominant perturbations in the deceleration region of

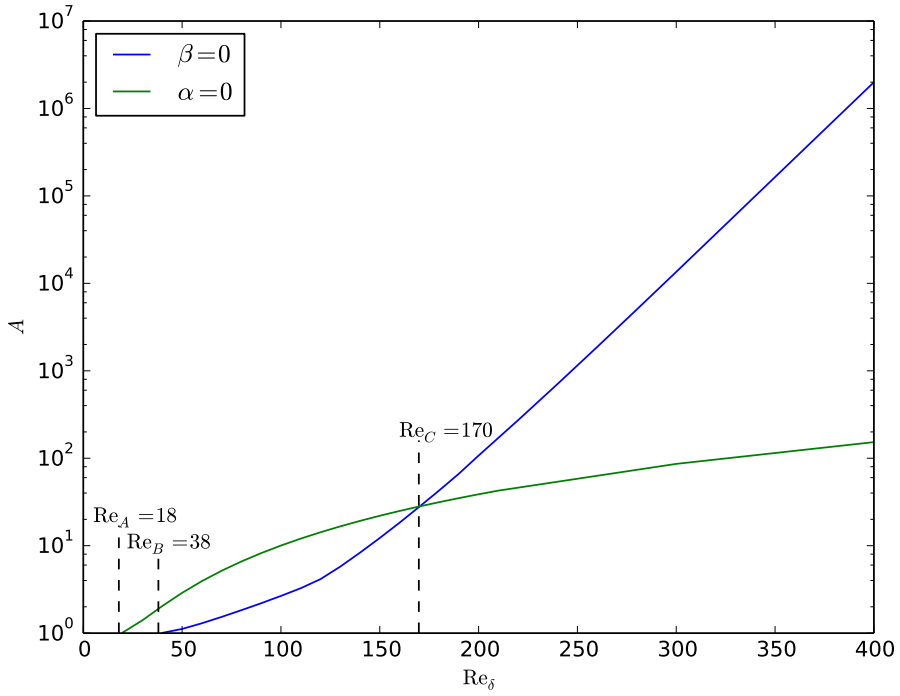

Figure 6: Maximum amplification of streamwise streaks $\max_{\beta,t_0,t} A(\alpha = 0, \beta, t_0, t, Re_\delta)$ and two-dimensional perturbations $\max_{\alpha,t_0,t} A(\alpha, \beta = 0, t_0, t, Re_\delta)$.

this flow are to be expected two-dimensional. This explains the findings in the direct numerical simulations by Vittori & Blondeaux (2008) and Ozdemir *et al.* (2013) and in the experiments by Sumer *et al.* (2010) of growing two-dimensional vortex rollers in the deceleration region of the flow. However, further investigation of the secondary instability mechanism and the receptivity to external (statistical) forcing is needed in order to explain the subsequent break-down to turbulence in the boundary layer.

Appendix A. Numerical implementation

A.1. *Numerical implementation for the energy bound*

We expand ζ and w in equations (2.20-2.21) on the Shen-Legendre polynomials ϕ_j and ψ_j for the Poisson and biharmonic operator, respectively, cf. (Shen 1994):

$$\zeta = \sum_{j=0}^{N-2} \zeta_j \phi_j(z) \quad w = \sum_{j=0}^{N-4} w_j \psi_j(z), \tag{A 1}$$

where N is the number of Legendre polynomials. The discrete system is then written as:

$$\begin{pmatrix} \mathbf{A} & \mathbf{B} \\ \mathbf{B}^T & \mathbf{D} \end{pmatrix} \begin{pmatrix} \mathbf{w} \\ \boldsymbol{\zeta} \end{pmatrix} = \mu \begin{pmatrix} \mathbf{E} & \mathbf{0} \\ \mathbf{0} & \mathbf{H} \end{pmatrix} \begin{pmatrix} \mathbf{w} \\ \boldsymbol{\zeta} \end{pmatrix} \tag{A 2}$$

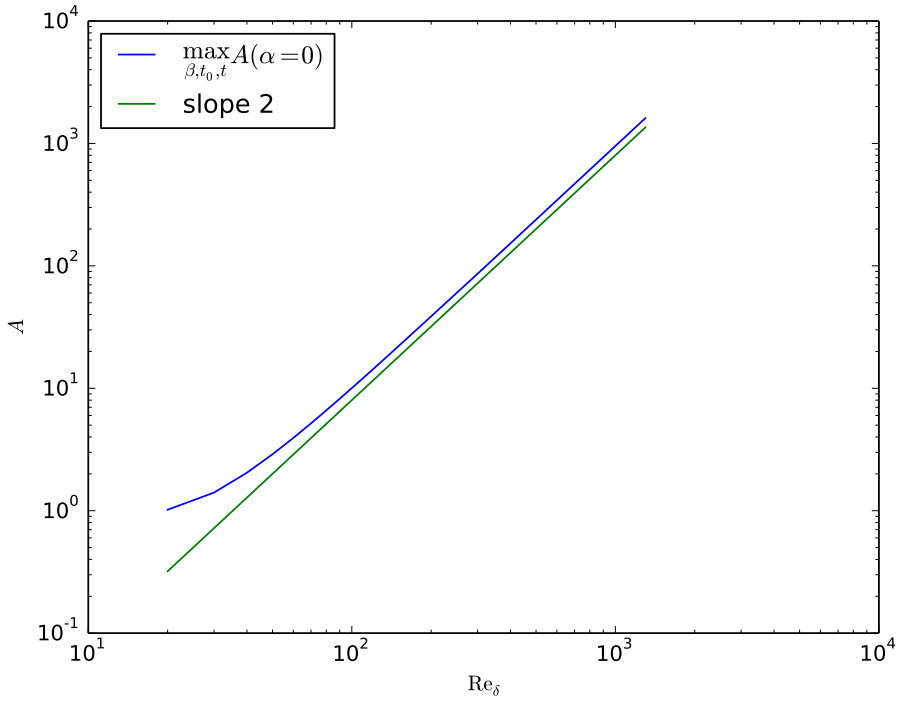

Figure 7: Maximum amplification of streamwise streaks, $\max_{\beta,t_0,t} A(\alpha = 0, \beta, t_0, t, Re_\delta)$, versus Reynolds number.

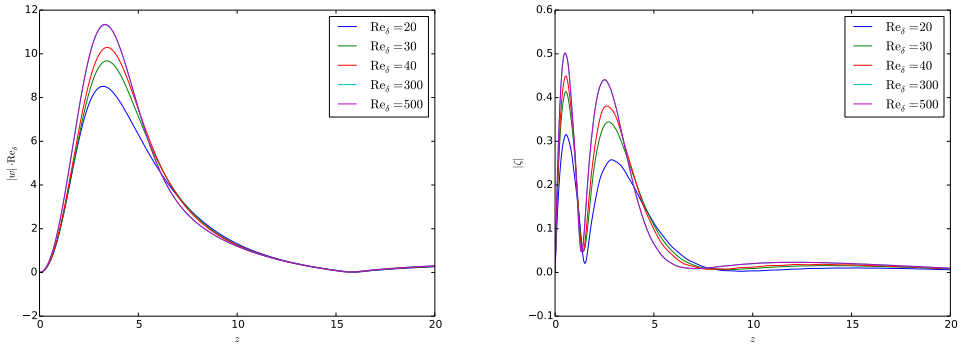

(a) w (b) ζ

Figure 8: Initial condition for the streamwise streak with maximum amplification, $\max_{\beta,t_0,t} A(\alpha = 0, \beta, t_0, t, Re_\delta)$, for different Reynolds numbers.

The elements of the matrices are given by:

$$A_{ij} = \frac{1}{Re}\left\{\int_0^h D^2\psi_i D^2\psi_j\,dz + 2\left(\alpha^2+\beta^2\right)\int_0^h D\psi_i D\psi_j\,dz + \left(\alpha^2+\beta^2\right)^2\int_0^h \psi_i\psi_j\,dz\right\}$$
$$+\frac{\mathrm{i}\alpha}{2}\left\{\int_0^h \psi_i\partial_z^2 U_{\mathrm{base}}\psi_j\,dz + 2\int_0^h \psi_i\partial_z U_{\mathrm{base}}\partial_z\psi_j\,dz\right\} \qquad \text{(A 3)}$$

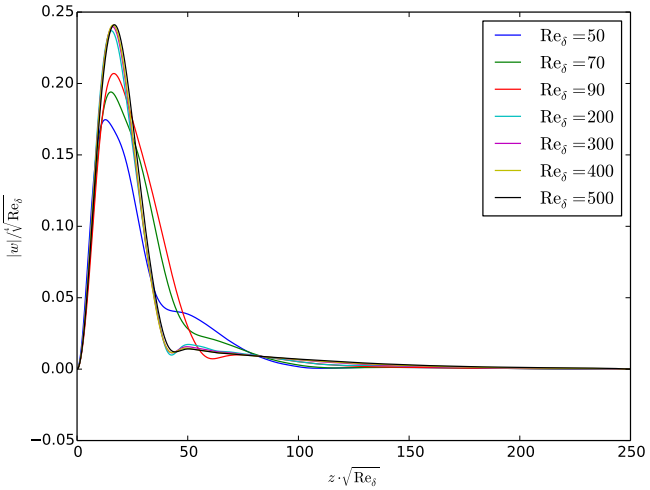

Figure 9: Initial condition w for the two-dimensional perturbations with maximum amplification, $\max_{\alpha,t_0,t} A(\alpha, \beta = 0, t_0, t, Re_\delta)$, for different Reynolds numbers.

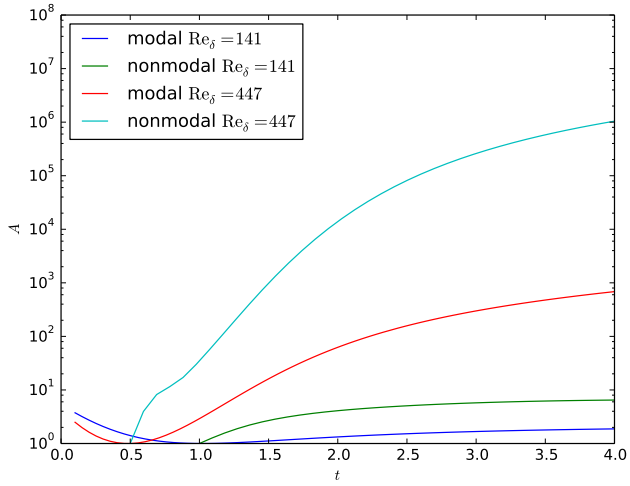

Figure 10: Amplification $A(\alpha = 0.35, \beta = 0, t_0, t, Re_\delta)$ of the nonmodal two-dimensional perturbation versus corresponding amplification of the modal Tollmien-Schlichting wave with $\alpha = 0.35$ computed by means of the Orr-Sommerfeld equation, for $Re_\delta = 141, 447$. The initial time t_0 is taken from the minimum of the modal Tollmien-Schlichting waves.

$$B_{ij} = \frac{\mathrm{i}\beta}{2} \int_0^h \psi_i \partial_z U_{\mathrm{base}} \phi_j \, dz \tag{A 4}$$

$$D_{ij} = \frac{1}{Re} \left\{ \int_0^h D\phi_i D\phi_j \, dz + \left(\alpha^2 + \beta^2\right) \int_0^h \phi_i \phi_j \, dz \right\} \tag{A 5}$$

$$2E_{ij} = -\int_0^h D\psi_i D\psi_j \, dz - \left(\alpha^2 + \beta^2\right) \int_0^h \psi_i \psi_j \, dz \tag{A 6}$$

$$2H_{ij} = -\int_0^h \phi_i \phi_j \, dz \tag{A 7}$$

For the verification and validation of the method, manufactured solutions have been used. In addition, the Reynolds numbers Re_A and Re_B for Stokes' second problem have been computed, resulting into $Re_A = 18.986$ and $Re_B = 38.951$, corresponding well with the numbers 19.0 and 38.9 obtained by Davis & von Kerczek (1973, table 1).

A.2. *Numerical implementation for the nonmodal analysis*

The basis functions ψ_j and ϕ_j for w and ζ are in this case given by the Shen-Chebyshev polynomials, cf. Shen (1995), instead of the Shen-Legendre polynomials as before. This allows us to use the fast Fourier transform for computing derivatives. The equations (2.24-2.25) are written in discrete form as:

$$\begin{pmatrix} \mathbf{L}^{\psi} & 0 \\ 0 & \mathbf{M}^{\phi} \end{pmatrix} \frac{d}{d\tau} \begin{pmatrix} \mathbf{w} \\ \boldsymbol{\zeta} \end{pmatrix} = \begin{pmatrix} \mathbf{L}^{OSE} & \mathbf{0} \\ \mathbf{L}^{C} & \mathbf{L}^{SC} \end{pmatrix} \begin{pmatrix} \mathbf{w} \\ \boldsymbol{\zeta} \end{pmatrix}, \tag{A 8}$$

where the elements of the matrices are given by:

$$M_{ij}^{\psi} = \int_0^h \psi_i \psi_j \, dz \tag{A 9}$$

$$G_{ij}^{\psi} = \int_0^h \frac{d}{dz}\psi_i \frac{d}{dz}\psi_j \, dz \tag{A 10}$$

$$A_{ij}^{\psi} = \int_0^h \frac{d^2}{dz^2}\psi_i \frac{d^2}{dz^2}\psi_j \, dz \tag{A 11}$$

$$M_{ij}^{\phi} = \int_0^h \phi_i \phi_j \, dz \tag{A 12}$$

$$G_{ij}^{\phi} = \int_0^h \frac{d}{dz}\phi_i \frac{d}{dz}\phi_j \, dz \tag{A 13}$$

$$P_{ij}^{1} = \int_0^h \partial_z^2 U_{\text{base}} \psi_i \psi_j \, dz \tag{A 14}$$

$$P_{ij}^{2} = \int_0^h U_{\text{base}} \psi_i \left(D^2 - (\alpha^2+\beta^2)\right) \psi_j \, dz \tag{A 15}$$

$$L_{ij}^{\psi} = -G_{ij}^{\psi} - (\alpha^2+\beta^2) M_{ij}^{\psi} \tag{A 16}$$

$$L_{ij}^{OSE} = \mathrm{i}\alpha P_{ij}^{1} - \mathrm{i}\alpha P_{ij}^{2} + \frac{1}{\mathrm{Re}}\left(A_{ij}^{\psi} + 2\left(\alpha^2+\beta^2\right) G_{ij}^{\psi} + \left(\alpha^2+\beta^2\right)^2 M_{ij}^{\psi}\right) \tag{A 17}$$

$$L_{ik}^{C} = \mathrm{i}\beta \int_0^h \partial_z U_0 \phi_i \psi_k \, dz \tag{A 18}$$

$$L_{ij}^{SC} = -\mathrm{i}\alpha P_{ij}^{3} + \frac{1}{\mathrm{Re}}\left(-G_{ij}^{\phi} - (\alpha^2+\beta^2) M_{ij}^{\phi}\right) \tag{A 19}$$

For the Shen-Chebyshev polynomials $\mathbf{L}^{\psi}$ and $\mathbf{M}^{\phi}$ are sparse band-diagonal matrices. Therefore, the system (A 2) can be efficiently advanced in time, allowing us to compute the evolution matrix $\mathbf{X}(\tau, \tau_0)$ for a wide range of parameters. The amplification A is then given by the square of the largest singular value of the matrix $\mathbf{Z}$, defined as in Trefethen *et al.* (1993); Schmid & Henningson (2001); Schmid (2007):

$$\mathbf{Z} = \mathbf{F}^{-1}\mathbf{C}\mathbf{X}\mathbf{B}\mathbf{F}, \tag{A 20}$$

where

$$\mathbf{C} = \begin{pmatrix} \frac{\mathrm{i}\alpha}{\alpha^2+\beta^2}\mathbf{M}^{-\phi}\mathbf{D}^{\phi\psi} & \frac{\mathrm{i}\beta}{\alpha^2+\beta^2}\mathbf{I} \\ \frac{\mathrm{i}\beta}{\alpha^2+\beta^2}\mathbf{M}^{-\phi}\mathbf{D}^{\phi\psi} & \frac{-\mathrm{i}\alpha}{\alpha^2+\beta^2}\mathbf{I} \\ \mathbf{I} & 0 \end{pmatrix}, \tag{A 21}$$

$$\mathbf{B} = \begin{pmatrix} -\mathrm{i}\alpha\mathbf{L}^{-\psi}\mathbf{D}^{\psi\phi} & -\mathrm{i}\beta\mathbf{L}^{-\psi}\mathbf{D}^{\psi\phi} & -\mathrm{i}\left(\alpha^2+\beta^2\right)\mathbf{L}^{-\psi}\mathbf{M}^{\psi} \\ -\mathrm{i}\beta\mathbf{I} & \mathrm{i}\alpha\mathbf{I} & 0 \end{pmatrix}. \tag{A 22}$$

Matrix $\mathbf{I}$ is the identity matrix and $\mathbf{D}^{\phi\psi}$ is given by

$$D_{ik}^{\phi\psi} = \int_0^h \phi_i \frac{d}{dz}\psi_j \, dz. \tag{A 23}$$

Matrix $\mathbf{F}$ results from a Cholesky factorization:

$$\mathbf{F}^T\mathbf{F} = \begin{pmatrix} \mathbf{M}^\phi & 0 & 0 \\ 0 & \mathbf{M}^\phi & 0 \\ 0 & 0 & \mathbf{M}^\psi \end{pmatrix}. \tag{A 24}$$

For the verification and validation of the method, manufactured solutions have been used.

REFERENCES

Aghsaee, P. , Boegman, L. , Diamessis, P. J. & Lamb, K. G. 2012 Boundary-layer-separation-driven vortex shedding beneath internal solitary waves of depression. *Journal of Fluid Mechanics* **690**, 321–344.

Andersson, P. , Brandt, L. , Bottaro, A. & Henningson, D. S. 2001 On the breakdown of boundary layer streaks. *Journal of Fluid Mechanics* **428**, 29–60.

Benjamin, T. B. 1966 Internal waves of finite amplitude and permanent form. *Journal of Fluid Mechanics* **25**, 241–270.

Blondeaux, P. , Pralits, J. & Vittori, G. 2012 Transition to turbulence at the bottom of a solitary wave. *Journal of Fluid Mechanics* **709**, 396–407.

Bogucki, D. , Dickey, T. & Redekopp, L. G. 1997 Sediment resuspension and mixing by resonantly generated internal solitary waves. *Journal of Physical Oceanography* **27**, 1181.

Brandt, L. , Schlatter, P. & Henningson, D. S. 2004 Transition in boundary layers subject to free-stream turbulence. *Journal of Fluid Mechanics* **517**, 167–198.

Butler, K. M. & Farrell, B. F. 1992 Three-dimensional optimal perturbations in viscous shear flow. *Physics of Fluids A* **4**, 1637–1650.

Carr, M. & Davies, P. A. 2006 The motion of an internal solitary wave of depression over a fixed bottom boundary in a shallow, two-layer fluid. *Physics of Fluids* **18**, 016601–10.

Carr, M. & Davies, P. A. 2010 Boundary layer flow beneath an internal solitary wave of elevation. *Physics of Fluids* **22**, 026601–1–8.

Corbett, P. & Bottaro, A. 2000 Optimal perturbations for boundary layers subject to stream-wise pressure gradient. *Physics of Fluids* **12** (1), 120–130.

Corbett, P. & Bottaro, A. 2001 Optimal linear growth in swept boudary layers. *Journal of Fluid Mechanics* **435**, 1–23.

Davis, S. H. & von Kerczek, C. 1973 A reformulation of energy stability theory. *Archive for Rational Mechanics and Analysis* pp. 112–117.

Diamessis, P. J. & Redekopp, L. G. 2006 Numerical investigation of solitary internal wave-induced global instability in shallow water benthic boundary layers. *Journa of Physical Oceanography* **36**, 784–811.

Drazin, P. G. & Reid, W. H. 1981 *Hydrodynamic Stability*. Cambridge University Press.

Fenton, J. 1972 A ninth-order solution for the solitary wave. *Journal of Fluid Mechanics* **53**, 257–271.

Gaster, M. 2016 Boundary layer transition initiated by a random excitation. In *Book of Abstracts* 24^{th} *International Congress of Theoretical and Applied Mechanics*.

Grimshaw, R. 1971 The solitary wave in water of variable depth. part 2. *Journal of Fluid Mechanics* **46**, 611–622.

Gustavsson, L. H. 1991 Energy growth of three-dimensional disturbances in plane Poiseuille flow. *Journal of Fluid Mechanics* **224**, 241–260.

von Kerczek, C. & Davis, S. H. 1974 Linear stability theory of oscillatory stokes layers. *Journal of Fluid Mechanics* **62**, 753–773.

Levin, O. & Henningson, D. S. 2003 Exponential vs algebra growth and transition prediction in boundary layer flow. *Flow, Turbulence and Combustion* **70**, 183–210.

Liu, P. L.-F. & Orfila, A. 2004 Viscous effects on transient long-wave propagation. *Journal of Fluid Mechanics* **520**, 83–92.

Liu, P. L.-F. , Park, Y. S. & Cowen, E. A. 2007 Boundary layer flow and bed shear stress under a solitary wave. *Journal of Fluid Mechanics* **574**, 449–463.

Luchini, P. & Bottaro, A. 2014 Adjoint equations in stability analysis. *Annual Review of Fluid Mechanics* **46**, 493–517.

Miles, J. W. 1980 Solitary waves. *Annual Review of Fluid Mechanics* **12**, 11–43.

Ozdemir, C. E. , Hsu, T.-J. & Balachandar, S. 2013 Direct numerical simulations of instability and boundary layer turbulence under a solitay wave. *Journal of Fluid Mechanics* **731**, 545–578.

Park, Y. S. , Verschaeve, J. C. G. , Pedersen, G. K. & Liu, P. L.-F. 2014 Corrigendum and addendum for boundary layer flow and bed shear stress under a solitary wave. *Journal of Fluid Mechanics* **753**, 554–559.

Schmid, P. J. 2007 Nonmodal stability theory. *Annual Review of Fluid Mechanics* **39**, 129–162.

Schmid, P. J. & Henningson, D. S. 2001 *Stability and Transition in Shear Flows*. New York: Springer-Verlag.

Shaikh, F. N. & Gaster, M. 1994 The non-linear evolution of modulated waves in a boundary layer. *Journal of Engineering Mathematics* **28**, 55–71.

Shen, J. 1994 Efficient spectral-galerkin method i. direct solvers for the second and fourth order equations using legendre polynomials. *Siam Journal of Scientific Coputing* **15**, 1489–1505.

Shen, J. 1995 Efficient spectral-galerkin method ii. direct solvers of second fourth order equations by using chebyshev polynomials. *SIAM Journal of Scientific Computing* **16** (1), 74–87.

Shuto, N. 1976 Transformation of nonlinear long waves. In *Proceedings of 15th Conference on Coastal Enginearing*.

Sumer, B. M. , Jensen, P. M. , Sørensen, L. B. , Fredsøe, J. , Liu, P. L.-F. & Carstensen, S. 2010 Coherent structures in wave boundary layers. part 2. solitary motion. *Journal of Fluid Mechanics* **646**, 207–231.

Trefethen, L. N. , Trefethen, A. E. , Reddy, S. C. & Driscoll, T. A. 1993 Hydrodynamic stability witwith eigenvalues. *Science* **261**, 578–584.

Verschaeve, J. C. G. & Pedersen, G. K. 2014 Linear stability of boundary layers under solitary waves. *Journal of Fluid Mechanics* **761**, 62–104.

Vittori, G. & Blondeaux, P. 2008 Turbulent boundary layer under a solitary wave. *Journal of Fluid Mechanics* **615**, 433–443.

Vittori, G. & Blondeaux, P. 2011 Characteristics of the boundary layer at the bottom of a solitary wave. *Coastal Engineering* **58**, 206–213.